

First-Principles Study of Hybrid Graphene and MoS₂ Nanocomposites

Wei Hu,^{1,2,*} Tian Wang,³ and Jinlong Yang^{2,†}

¹*Computational Research Division, Lawrence Berkeley National Laboratory, Berkeley, CA 94720, USA*

²*Hefei National Laboratory for Physical Sciences at Microscale,
and Synergetic Innovation Center of Quantum Information and Quantum Physics,
University of Science and Technology of China, Hefei, Anhui 230026, China*

³*Department of Precision Machinery and Precision Instrumentation,
University of Science and Technology of China, Hefei, Anhui 230026, China*

(Dated: November 4, 2014)

Combining the electronic properties of graphene and molybdenum disulphide (MoS₂) monolayers in two-dimensional (2D) ultrathin hybrid nanocomposites have been synthesized experimentally to create excellent electronic, electrochemical, photovoltaic, photoresponsive and memory devices. Here, first-principles calculations are performed to investigate the electronic, electrical and optical properties in hybrid G/MoS₂ and G/MoS₂/G nanocomposites. It turns out that weak van der Waals interactions dominate between graphene and MoS₂ with their intrinsic electronic properties preserved. Interestingly, tunable p-type doping of graphene is very easy to achieve by applying electric fields perpendicular to hybrid G/MoS₂ and G/MoS₂/G nanocomposites, because electrons can easily transfer from the Dirac point of graphene to the conduction band of MoS₂ due to the work function of graphene close to the electronic affinity of MoS₂. Vertical electric fields can generate strong p-type but weak n-type doping of graphene, inducing electron-hole pairs in hybrid G/MoS₂/G sandwiched nanocomposites. Moreover, improved optical properties in hybrid G/MoS₂ and G/MoS₂/G nanocomposites are also expected with potential photovoltaic and photoresponsive applications.

INTRODUCTION

Graphene, a two-dimensional (2D) sp²-hybridized carbon sheet, has received considerable interest recently owing to its outstanding properties,[1–4] especially, high carrier mobility, with great potential applications for graphene-based electronic devices, such as field effect transistors (FETs). But, intrinsic electronic properties of graphene depend sensitively on the substrates due to strong graphene-substrate interactions, such as SiO₂,[5–7] SiC,[8–10] and metal surfaces.[11–13] Finding an ideal substrate for graphene remains a significant challenge.

Interestingly, many 2D ultrathin hybrid graphene-based nanocomposites have been widely studied experimentally and theoretically, such as graphene/hexagonal boron nitride (G/h-BN),[14–16] graphene/graphitic carbon nitride (G/g-C₃N₄),[17–19] and graphene/graphitic ZnO (G/g-ZnO).[20–22] These hybrid graphene-based nanocomposites show much more new properties far beyond their simplex components. Furthermore, most of them are ideal substrates for graphene to preserve its intrinsic electronic properties.

Recently, 2D flexible heterostructures consisting of graphene and monolayer molybdenum disulphide[23–27] (G/MoS₂) have been synthesized experimentally[28–37] with great applications in excellent electronic, electrochemical, photovoltaic, photoresponsive and memory devices. Monolayer MoS₂ itself is an interesting semiconducting transition metal dichalcogenide, which has been widely studied experimentally and theoretically[23–27] due to its outstanding structural, electronic and optical properties superior to other 2D materials as graphene

substrates. For example, monolayer MoS₂ has a appropriate bandgap (1.90 eV)[24] to achieve a high current on/off ratio of 10000 in G/MoS₂ based FETs far superior to vertical G/h-BN heterostructures with an insufficient current on/off ratio of 50 due to the large bandgap (5.97 eV) of h-BN.[30] Most recently, hybrid G/MoS₂/G sandwiched nanocomposites have also been synthesized experimentally,[38, 39] showing strong light-matter interactions and large quantum tunneling current modulations in flexible graphene-based FETs superior to hybrid G/MoS₂ nanocomposites. Theoretically, only few works[40, 41] have been focused on the structural and electronic of hybrid G/MoS₂ nanocomposites. Therefore, a systematic theoretical work on hybrid graphene and MoS₂ nanocomposites (G/MoS₂ and G/MoS₂/G) is very desirable with more exciting new properties to be expected, such as electrical and optical properties.

In the present work, we study structural, electronic, electrical and optical properties in hybrid G/MoS₂ and G/MoS₂/G nanocomposites using first-principles calculations. Graphene interacts overall weakly with via van der Waals interactions with their intrinsic electronic properties preserved. Applying vertical electric fields is very easy to induce tunable p-type doping of graphene in hybrid G/MoS₂ nanocomposites and generate strong p-type but weak n-type doping of graphene in hybrid G/MoS₂/G sandwiched nanocomposites. Moreover, hybrid graphene and MoS₂ nanocomposites show enhanced optical absorption compared to simplex graphene and MoS₂ monolayers.

THEORETICAL MODELS AND METHODS

The lattice parameters of graphene and MoS₂ monolayers calculated to setup unit cell are $a(\text{G}) = 2.47 \text{ \AA}$ and $a(\text{MoS}_2) = 3.19 \text{ \AA}$. [40, 41] In order to simulate hybrid graphene and MoS₂ nanocomposites, a $2\sqrt{3} \times 2\sqrt{3}$ supercell of graphene (24 carbon atoms) is used to match a $\sqrt{7} \times \sqrt{7}$ supercell of MoS₂ (7 sulfur and 14 molybdenum atoms) with a smaller lattice mismatch of about 1% compared with previous theoretical studies. [40, 41] Furthermore, our designed hybrid graphene and MoS₂ nanocomposites are consistent with recent experimental observation of a faint moiré structure with high resolution STM images of graphene on MoS₂. [37] In this work, both hybrid G/MoS₂ and G/MoS₂/G nanocomposites are considered as shown in FIG 1. The vacuum space in the Z direction is about 15 Å to separate the interactions between neighboring slabs.

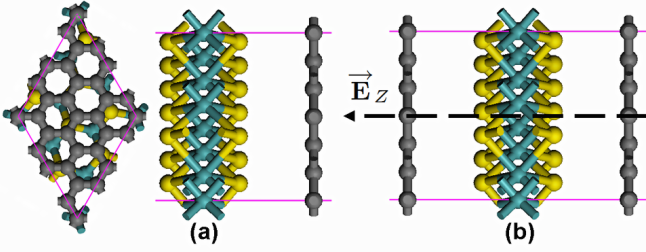


FIG. 1: (Color online) Atomic geometries of hybrid (a) G/MoS₂ and (b) G/MoS₂/G nanocomposites. A vertical electric field is applied perpendicular to the layers. The gray, yellow and blue balls denote carbon, sulfur and molybdenum atoms, respectively.

First-principles calculations are based on the density functional theory (DFT) implemented in the VASP package. [42] The generalized gradient approximation of Perdew, Burke, and Ernzerhof (GGA-PBE) [43] with van der Waals (vdW) correction proposed by Grimme (DFT-D2) [44] is chosen due to its good description of long-range vdW interactions. [45–56] As a benchmark, DFT-D2 calculations give a good bilayer distance of 3.25 Å and binding energy of -25 meV per carbon atom for bilayer graphene, fully agreeing with previous experimental [57, 58] and theoretical [59, 60] studies. The energy cutoff is set to be 500 eV. The surface Brillouin zone is sampled with a 5×5 regular mesh and 240 k points are used for calculating the tiny band gaps at the Dirac points of silicene. All the geometry structures are fully relaxed until energy and forces are converged to 10^{-5} eV and 0.01 eV/\AA , respectively. Dipole correction is employed to cancel the errors of electrostatic potential, atomic forces and total energy, caused by periodic boundary condition. [61] The external electric field is introduced in the VASP by the dipole layer method with the dipole

placed in the vacuum region of periodic supercell.

To study the optical properties of hybrid graphene and MoS₂ nanocomposites, the frequency-dependent dielectric matrix is calculated. [62] The imaginary part of dielectric matrix is determined by a summation over states as

$$\varepsilon''_{\alpha\beta} = \frac{4\pi^2 e^2}{\Omega} \lim_{q \rightarrow 0} \frac{1}{q^2} \sum_{c,v,\mathbf{k}} 2w_{\mathbf{k}} \delta(\epsilon_{c\mathbf{k}} - \epsilon_{v\mathbf{k}} - \omega) \times \langle \mu_{c\mathbf{k}+\mathbf{e}_\alpha q} | \mu_{v\mathbf{k}} \rangle \langle \mu_{c\mathbf{k}+\mathbf{e}_\beta q} | \mu_{v\mathbf{k}} \rangle^* \quad (1)$$

where, Ω is the volume of the primitive cell, $w_{\mathbf{k}}$ is the \mathbf{k} point weight, c and v are the conduction and valence band states respectively, $\epsilon_{c\mathbf{k}}$ and $\mu_{c\mathbf{k}}$ are the eigenvalues and wavefunctions at the \mathbf{k} point respectively, and \mathbf{e}_α are the unit vectors for the three Cartesian directions. In order to accurately calculate the optical properties of hybrid graphene and MoS₂ nanocomposites, a large 21×21 regular mesh for the surface Brillouin zone, a large number of empty conduction band states (three times more than the number of valence band) and frequency grid points (4000) are adopted. Note that the optical properties of pristine graphene and MoS₂ monolayers are crosschecked and consistent with previous theoretical calculations. [63, 64]

In order to evaluate the stability of hybrid graphene and MoS₂ nanocomposites, the interface binding energy is defined as

$$E_b = E(\text{G/MoS}_2) - E(\text{G}) - E(\text{MoS}_2) \quad (2)$$

where, $E(\text{G/MoS}_2)$, $E(\text{G})$ and $E(\text{MoS}_2)$ represent the total energy of hybrid graphene and MoS₂ nanocomposites, pristine graphene and MoS₂ monolayers, respectively.

RESULTS AND DISCUSSION

First, we check the structural and electronic properties of pristine graphene and MoS₂ monolayers, agreeing well with previous theoretical studies. [40, 41] Pristine graphene monolayer is a zero-gap semiconductor, showing a linear Dirac-like dispersion relation $E(k) = \pm \hbar \nu_F |k|$ around the Fermi level, where ν_F is the Fermi velocity, and $\nu_F(\text{G}) = 0.8 \times 10^6 \text{ m/s}$ [63] at the Dirac point of graphene, although GGA-PBE calculations underestimate the Fermi velocity of graphene by 15~20%. [65] Pristine MoS₂ monolayer is a semiconductor with a direct band gap of 1.64 eV, although GGA-PBE calculations [66] slightly underestimate this band gap value (1.90 eV). [24]

We then study the structural and electronic properties of hybrid graphene and MoS₂ nanocomposites as summarized in TABLE I. The equilibrium spacings of 3.37 and 3.36 Å are obtained for hybrid G/MoS₂ and G/MoS₂/G

TABLE I: DFT-D2 calculated equilibrium interfacial distance D_0 (Å) and binding energy per carbon atom E_b (meV) in hybrid G/MoS₂ and G/MoS₂/G nanocomposites.

DFT-D2	D_0	E_b
G/MoS ₂	3.37	-20.5
G/MoS ₂ /G	3.36/3.36	-27.0

nanocomposites with corresponding binding energy of -20.5 and 27.0 meV per atom, respectively. Thus, graphene is physically adsorbed on monolayer MoS₂ via weak van der Waals (vdW) interactions, and intrinsic electronic properties of graphene and MoS₂ can be preserved in ultrathin hybrid nanocomposites, agreeing well with previous experimental[28–39] and theoretical[40, 41] studies.

Electronic band structures of hybrid graphene and MoS₂ nanocomposites are shown as FIG 2. We find that linear Dirac-like dispersion relation around the Fermi levels of graphene is still preserved in hybrid G/MoS₂ and G/MoS₂/G nanocomposites, though tiny band gaps (1 meV) are opened at the Dirac points of graphene, which are significantly lower than thermal fluctuation (about 25 meV) at room temperature and trend to vanish in experiments. Note that induced graphene band gaps are typically sensitive to other external conditions, such as interlayer separation,[63] showing that the band gap values increase gradually with the interlayer separation decrease, thus tunable, with a potential for flexible graphene-based FETs.

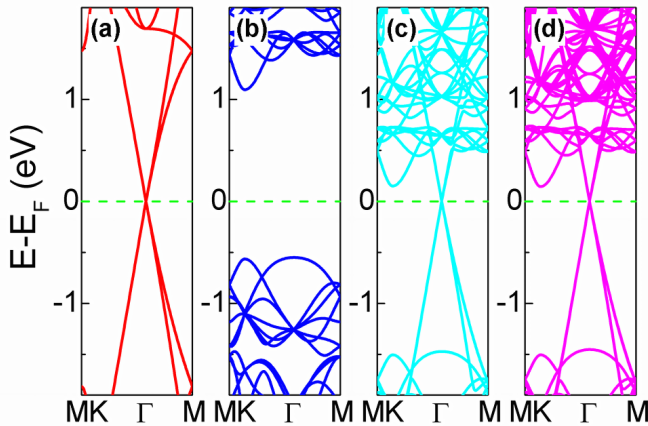


FIG. 2: (Color online) Electronic band structures of (a) graphene and (b) MoS₂ as well as corresponding hybrid (c) G/MoS₂ and (d) G/MoS₂/G nanocomposites. The Fermi level is set to zero and marked by green dotted lines.

High-performance field-effect tunneling transistors have been achieved experimentally[30, 34, 36, 38, 39] in hybrid graphene and MoS₂ nanocomposites. Thus, the

electronic properties of hybrid G/MoS₂ and G/MoS₂/G nanocomposites affected by applying vertical electric fields are very desirable as shown in FIG 3. Interestingly, negative vertical electric fields can induce p-type doping of graphene in hybrid G/MoS₂ nanocomposites. But, positive electric fields almost have no effect on the electronic properties of hybrid G/MoS₂ nanocomposites. This is because electrons can easily move from the Dirac point of graphene to the conduction band of MoS₂ but difficulty from the valence band of MoS₂ to the Dirac point of graphene due to the work function (4.3 eV)[20] of graphene close to the electronic affinity (4.2 eV)[34] of monolayer MoS₂. Interestingly, vertical electric fields can generate strong p-type but weak n-type doping of graphene at both negative and positive electric fields due to the symmetry in hybrid G/MoS₂/G nanocomposites. Based on the linear dispersion around the Dirac point of graphene,[3] the charge carrier (hole or electron) concentration of doped graphene can be estimated by the following equation[20]

$$N_{h/e} = \frac{(\Delta E_D)^2}{\pi(\hbar v_F)^2} \quad (3)$$

where ΔE_D is the shift of graphene's Dirac point (E_D) relative to the Fermi level (E_F), that is $\Delta E_D = E_D - E_F$. The calculated charge carrier concentrations in hybrid G/MoS₂ and G/MoS₂/G nanocomposites are shown in FIG 4. These values are more than 3 orders of magnitude larger than the intrinsic charge carrier concentration of graphene at room temperature ($n = \pi k_B^2 T^2 / 6 \hbar v_F^2 = 6 \times 10^{10} \text{ cm}^{-2}$).[10] Furthermore, the doping charge carrier concentrations of graphene in hybrid nanocomposites are increased with the vertical electric fields. Therefore, the field-effect in hybrid graphene and MoS₂ nanocomposites is effective and tunable for high-performance FETs and p-n junctions.[38, 39]

As an example, electronic band structures of hybrid G/MoS₂ and G/MoS₂/G nanocomposites and their corresponding XY-averaged electrostatic potential (V) in the Z direction at a vertical electric field of -2.0 V/Å are shown in FIG 4. Charge-transfer complexes are formed in hybrid graphene and MoS₂ nanocomposites affected by vertical electric fields. The differential charge density ($\Delta\rho = \rho(\text{G/MoS}_2) - \rho(\text{G}) - \rho(\text{MoS}_2)$) of hybrid G/MoS₂ and G/MoS₂/G nanocomposites are shown in FIG 3c. Particularly, electron-hole pairs are well separated in hybrid G/MoS₂/G sandwiched nanocomposites with more excellent applications[38, 39] compared with hybrid G/MoS₂ nanocomposites. Note that the band gap values at graphene's Dirac points in hybrid G/MoS₂ and G/MoS₂/G nanocomposites are almost not affected by vertical electric fields, different to bilayer graphene.[67, 68]

Besides commonly focused electronic structures in hybrid G/MoS₂ nanocomposites,[40, 41] we also study the optical properties in hybrid G/MoS₂ and G/MoS₂/G

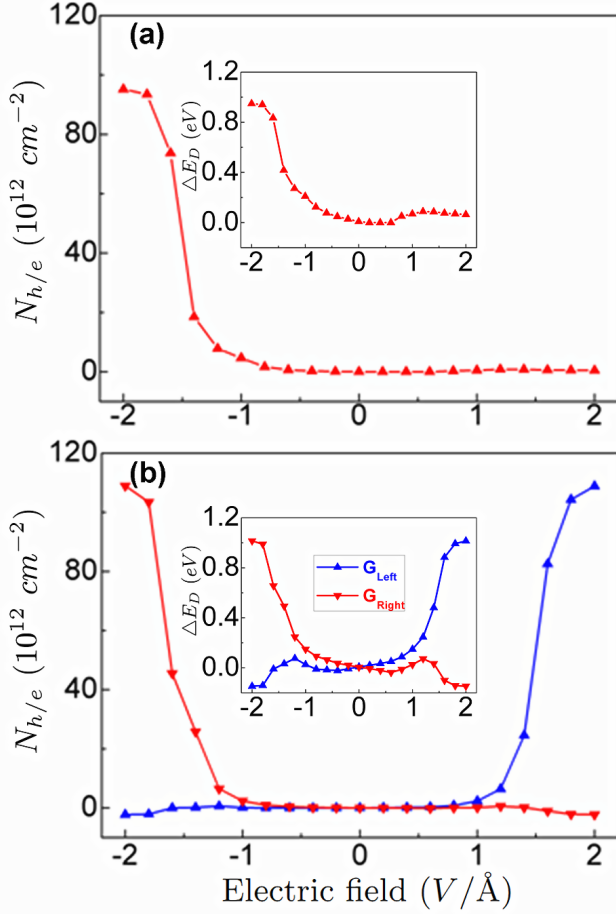


FIG. 3: (Color online) The doping charge carrier concentrations $N_{h/e}$ (10^{12} cm^{-2}) of graphene in hybrid G/MoS₂ and G/MoS₂/G nanocomposites as a function of vertical electric field E ($\text{V}/\text{\AA}$). The energy shift ΔE_D (eV) of graphene's Dirac point relative to the Fermi level is shown in the inset.

nanocomposites due to their photovoltaic and photore sponsive applications.[35–38] Note that pristine graphene and MoS₂ monolayers themselves display outstanding optical properties,[4, 25] but interlayer interaction and charge transfer in graphene-based hybrid nanocomposites can induce new optical transitions.[19] In optical property calculations, the imaginary part of dielectric function for pristine graphene and MoS₂ monolayers as well as corresponding hybrid graphene and MoS₂ nanocomposites are evaluated as shown in FIG 5. In fact, monolayer MoS₂ shows much stronger optical absorption than graphene in the visible light region ($200 \sim 800 \text{ nm}$). Moreover, hybrid graphene and MoS₂ nanocomposites exhibit more strongly enhanced light response, especially hybrid G/MoS₂/G sandwiched heterostructures, compared with simplex graphene and MoS₂ monolayers, because electrons can now be easily and directly excited

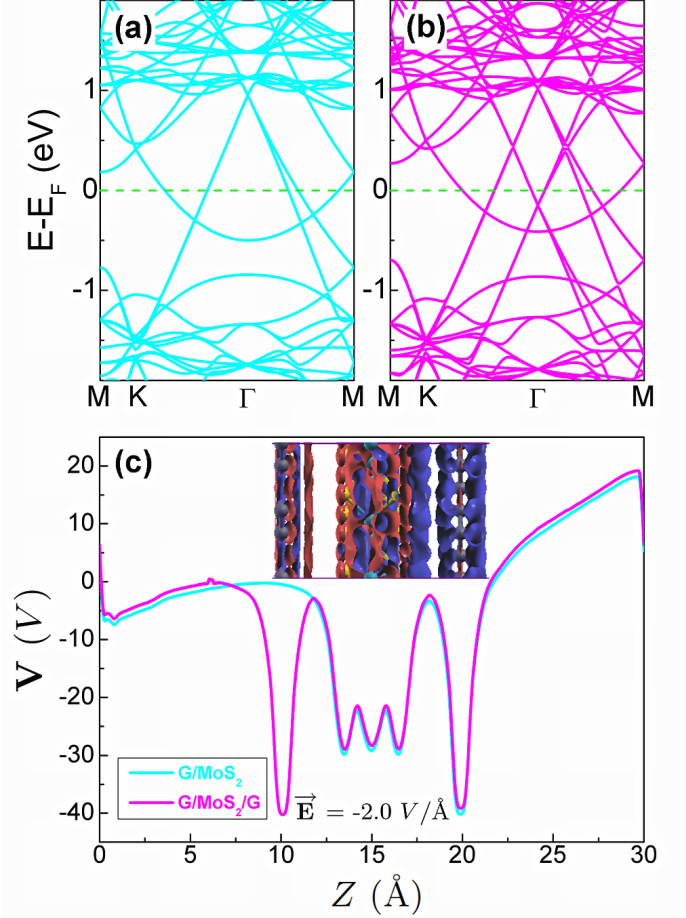


FIG. 4: (Color online) Electronic band structures of hybrid (a) G/MoS₂ and (b) G/MoS₂/G nanocomposites and (c) their corresponding XY-averaged electrostatic potential V (V) in the Z (\AA) direction at a vertical electric field of $-2.0 \text{ V}/\text{\AA}$. Differential charge density with a isosurface value of $0.001 \text{ e}/\text{\AA}^3$ of hybrid G/MoS₂/G nanocomposites is shown in the insert. The red and blue regions indicate electron increase and decrease, respectively.

from the Dirac point of graphene to the conduction band of MoS₂.

SUMMARY AND CONCLUSIONS

In summary, structural, electronic, electrical and optical properties in hybrid G/MoS₂ and G/MoS₂/G nanocomposites are studied via first-principles calculations. Graphene interacts overall weakly with via van der Waals interactions with their intrinsic electronic properties preserved. Applying vertical electric fields is very easy to induce tunable p-type doping of graphene in hybrid G/MoS₂ nanocomposites and generate p-type and n-type doping of graphene in hybrid G/MoS₂/G

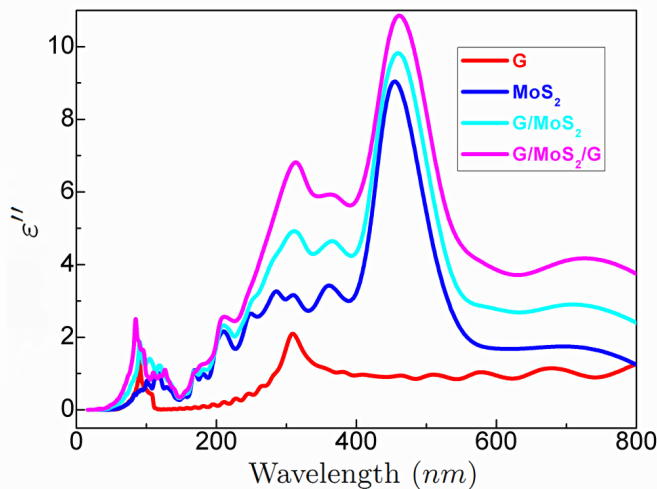


FIG. 5: (Color online) Imaginary part of dielectric function (ϵ'') of pristine graphene MoS_2 monolayers as well as corresponding hybrid G/MoS_2 and $\text{G}/\text{MoS}_2/\text{G}$ nanocomposites.

sandwiched nanocomposites. Moreover, hybrid G/MoS_2 and $\text{G}/\text{MoS}_2/\text{G}$ nanocomposites display enhanced optical absorption compared to simplex graphene and MoS_2 monolayers. With excellent electronic, electrical and optical properties combined, ultrathin hybrid graphene and MoS_2 nanocomposites are expected to be with great applications in efficient electronic, electrochemical, photovoltaic, photoresponsive and memory devices.

ACKNOWLEDGMENTS

This work is partially supported by the National Key Basic Research Program (2011CB921404), by NSFC (21121003, 91021004, 2123307, 21222304), by CAS(XDB01020300). This work is also partially supported by the Scientific Discovery through Advanced Computing (SciDAC) program funded by U.S. Department of Energy, Office of Science, Advanced Scientific Computing Research and Basic Energy Sciences (W. H.). We thank the National Energy Research Scientific Computing (NERSC) center, and the USTCSCC, SC-CAS, Tianjin, and Shanghai Supercomputer Centers for the computational resources.

* Corresponding author. E-mail: whu@lbl.gov

† Corresponding author. E-mail: jlyang@ustc.edu.cn

[1] K. S. Novoselov, A. K. Geim, S. V. Morozov, D. Jiang, Y. Zhang, S. V. Dubonos, I. V. Grigorieva, and A. A. Firsov, *Science* **306**, 666 (2004).

- [2] A. K. Geim and K. S. Novoselov, *Nature Mater.* **6**, 183 (2007).
- [3] A. H. C. Neto, F. Guinea, N. M. R. Peres, K. S. Novoselov, and A. K. Geim, *Rev. Mod. Phys.* **81**, 109 (2009).
- [4] F. Bonaccorso, Z. Sun, T. Hasan, and A. C. Ferrari, *Nature Photon.* **4**, 611 (2010).
- [5] M. Ishigami, J. H. Chen, W. G. Cullen, M. S. Fuhrer, and E. D. Williams, *Nano Lett.* **7**, 1643 (2007).
- [6] J. Martin, N. Akerman, G. Ulbricht, T. Lohmann, J. H. Smet, K. von Klitzing, and A. Yacoby, *Nature Phys.* **4**, 144 (2008).
- [7] N. T. Cuong, M. Otani, and S. Okada, *Phys. Rev. Lett.* **106**, 106801 (2011).
- [8] S. Y. Zhou, G.-H. Gweon, A. V. Fedorov, P. N. First, W. A. de Heer, D.-H. Lee, F. Guinea, A. H. C. Neto, and A. Lanzara, *Nature Mater.* **6**, 770 (2007).
- [9] F. Varchon, R. Feng, J. Hass, X. Li, B. N. Nguyen, C. Naud, P. Mallet, J.-Y. Veuillen, C. Berger, E. H. Conrad, and L. Magaud, *Phys. Rev. Lett.* **99**, 126805 (2007).
- [10] J. Ristein, S. Mammadov, and T. Seyller, *Phys. Rev. Lett.* **108**, 246104 (2012).
- [11] G. Giovannetti, P. A. Khomyakov, G. Brocks, V. M. Karpan, J. van den Brink, and P. J. Kelly, *Phys. Rev. Lett.* **101**, 026803 (2008).
- [12] P. A. Khomyakov, G. Giovannetti, P. C. Rusu, G. Brocks, J. van den Brink, and P. J. Kelly, *Phys. Rev. B* **79**, 195425 (2009).
- [13] F. Xia, V. Perebeinos, Y. Lin, Y. Wu, and P. Avouris, *Nature Nanotech.* **6**, 179 (2011).
- [14] C. R. Dean, A. F. Young, I. Meric, C. Lee, L. Wang, S. Sorgenfrei, K. Watanabe, T. Taniguchi, P. Kim, K. L. Shepard, and J. Hone, *Nature Nanotech.* **5**, 722 (2010).
- [15] J. Xue, J. Sanchez-Yamagishi, D. Bulmash, P. Jacquod, A. Deshpande, K. Watanabe, T. Taniguchi, P. Jarillo-Herrero, and B. LeRoy, *Nature Mater.* **10**, 282 (2011).
- [16] K. H. Lee, H.-J. Shin, J. Lee, I. Lee, G.-H. Kim, J.-Y. Choi, and S.-W. Kim, *Nano Lett.* **12**, 714 (2012).
- [17] Q. J. Xiang, J. G. Yu, and M. Jaroniec, *J. Phys. Chem. C* **115**, 7355 (2011).
- [18] X.-H. Li, J.-S. Chen, X. Wang, J. Sun, and M. Antonietti, *J. Am. Chem. Soc.* **133**, 8074 (2011).
- [19] A. Du, S. Sanvito, Z. Li, D. Wang, Y. Jiao, T. Liao, Q. Sun, Y. H. Ng, Z. Zhu, R. Amal, and S. C. Smith, *J. Am. Chem. Soc.* **134**, 4393 (2012).
- [20] W. Hu, Z. Li, and J. Yang, *J. Chem. Phys.* **138**, 124706 (2013).
- [21] W. Geng, X. Zhao, H. Liu, and X. Yao, *J. Phys. Chem. C* **117**, 10536 (2013).
- [22] X. Guo and Y. G. Zhou, *J. Appl. Phys.* **113**, 054307 (2013).
- [23] M. V. Bollinger, J. V. Lauritsen, K. W. Jacobsen, J. K. Nørskov, S. Helveg, and F. Besenbacher, *Phys. Rev. Lett.* **87**, 196803 (2001).
- [24] K. F. Mak, C. Lee, J. Hone, J. Shan, and T. F. Heinz, *Phys. Rev. Lett.* **105**, 136805 (2010).
- [25] A. Splendiani, L. Sun, Y. Zhang, T. Li, J. Kim, C.-Y. Chim, G. Galli, and F. Wang, *Nano Lett.* **10**, 1271 (2010).
- [26] B. Radisavljevic, A. Radenovic, J. Brivio, V. Giacometti, and A. Kis, *Nature Nanotech.* **6**, 147 (2011).
- [27] Z. Yin, H. Li, H. Li, L. Jiang, Y. Shi, Y. Sun, G. Lu, Q. Zhang, X. Chen, and H. Zhang, *ACS Nano* **6**, 74 (2012).
- [28] K. Chang and W. Chen, *Chem. Commun.* **47**, 4252 (2007).

- (2011).
- [29] K. Chang and W. Chen, ACS Nano **5**, 4720 (2011).
 - [30] L. Britnell, R. V. Gorbachev, R. Jalil, B. D. Belle, F. Schedin, A. Mishchenko, T. Georgiou, M. I. Katsnelson, L. Eaves, S. V. Morozov, N. M. R. Peres, J. Leist, A. K. Geim, K. S. Novoselov, and L. A. Ponomarenko, Science **335**, 947 (2012).
 - [31] Y. Shi, W. Zhou, A.-Y. Lu, W. Fang, Y.-H. Lee, A. L. Hsu, S. M. Kim, K. K. Kim, H. Y. Yang, L.-J. Li, J.-C. Idrobo, and J. Kong, Nano Lett. **12**, 2784 (2012).
 - [32] Q. Xiang, J. Yu, and M. Jaroniec, J. Am. Chem. Soc. **134**, 6575 (2012).
 - [33] W. J. Yu, Z. Li, H. Zhou, Y. Chen, Y. Wang, Y. Huang, X. Duan, X. Nature Mater. **12**, 246 (2013).
 - [34] M. S. Choi, G. H. Lee, Y. J. Yu, D. Y. Lee, S. H. Lee, P. Kim, J. Hone, and W. J. Yoo, Nature Commun. **4**, 1624 (2013).
 - [35] S. Bertolazzi, D. Krasnozhan, and A. Kis, ACS Nano **7**, 3246 (2013).
 - [36] K. Roy, M. Padmanabhan, S. Goswami, T. P. Sai, G. Ramalingam, S. Raghavan, and A. Ghosh, Nature Nanotech. **8**, 826 (2013).
 - [37] H. Diaz, R. Addou, and M. Batzill, Nanoscale **6**, 1071 (2014).
 - [38] L. Britnell, R. M. Ribeiro, A. Eckmann, R. Jalil, B. D. Belle, A. Mishchenko, Y.-J. Kim, R. V. Gorbachev, T. Georgiou, S. V. Morozov, A. N. Grigorenko, A. K. Geim, C. Casiraghi, A. H. C. Neto, K. S. Novoselov, Science **340**, 1311 (2013).
 - [39] N. Myoung, K. Seo, S. J. Lee, and G. Ihm, ACS Nano **7**, 7021 (2013).
 - [40] Y. Ma, Y. Dai, M. Guo, C. Niu, and B. Huang, Nanoscale **3**, 3883 (2011).
 - [41] X. D. Li, S. Yu, S. Q. Wu, Y. H. Wen, S. Zhou, and Z. Z. Zhu, J. Phys. Chem. C **117**, 15347 (2013).
 - [42] G. Kresse and J. Hafner, Phys. Rev. B **47**, 558 (1993).
 - [43] J. P. Perdew, K. Burke, and M. Ernzerhof, Phys. Rev. Lett. **77**, 3865 (1996).
 - [44] S. Grimme, J. Comput. Chem. **27**, 1787 (2006).
 - [45] S. Grimme, C. Muck-Lichtenfeld, and J. Antony, J. Phys. Chem. C **111**, 11199 (2007).
 - [46] J. Antony and S. Grimme, Phys. Chem. Chem. Phys. **10**, 2722 (2008).
 - [47] N. Kharche and S. K. Nayak, Nano Lett. **11**, 5274 (2011).
 - [48] J. Ślawińska, P. Dabrowski, and I. Zasada, Phys. Rev. B **83**, 245429 (2011).
 - [49] R. Kagimura, M. S. C. Mazzoni, and H. Chacham, Phys. Rev. B **85**, 125415 (2012).
 - [50] Y. Ma, Y. Dai, M. Guo, and B. Huang, Phys. Rev. B **85**, 235448 (2012).
 - [51] L. Yuan, Z. Li, J. Yang, and J. G. Hou, Phys. Chem. Chem. Phys. **14**, 8179 (2012).
 - [52] L. Yuan, Z. Li, and J. Yang, Phys. Chem. Chem. Phys. **15**, 497 (2013).
 - [53] W. Hu, X. Wu, Z. Li, and J. Yang, Phys. Chem. Chem. Phys. **15**, 5753 (2013).
 - [54] W. Hu, X. Wu, Z. Li, and J. Yang, Nanoscale **5**, 9062 (2013).
 - [55] L. Chen, L. Wang, Z. Shuai, and D. Beljonne, J. Phys. Chem. Lett. **4**, 2158 (2013).
 - [56] W. Hu, N. Xia, X. Wu, Z. Li, and J. Yang, Phys. Chem. Chem. Phys. (2014).
 - [57] Y. Baskin and L. Mayer, Phys. Rev. **100**, 544 (1955).
 - [58] R. Zacharia, H. Ulbricht, and T. Hertel, Phys. Rev. B **69**, 155406 (2004).
 - [59] R. E. Mapasha, A. M. Ukpong, and N. Chetty, Phys. Rev. B **85**, 205402 (2012).
 - [60] W. Hu, Z. Li, and J. Yang, J. Chem. Phys. **138**, 054701 (2013).
 - [61] G. Makov and M. C. Payne, Phys. Rev. B **51**, 4014 (1995).
 - [62] M. Gajdoš, K. Hummer, and G. Kresse, Phys. Rev. B **73**, 045112 (2006).
 - [63] W. Hu, Z. Li, and J. Yang, J. Chem. Phys. **139**, 154704 (2013).
 - [64] A. Molina-Sánchez, D. Sangalli, K. Hummer, A. Marini, and L. Wirtz, Phys. Rev. B **88**, 045412 (2013).
 - [65] M. Calandra and F. Mauri, Phys. Rev. B **76**, 205411 (2007).
 - [66] S. Lany and A. Zunger, Phys. Rev. B **78**, 235104 (2008).
 - [67] Y. Zhang, T.-T. Tang, C. Girit, Z. Hao, M. C. Martin, A. Zettl, M. F. Crommie, Y. R. Shen, and F. Wang, Nature **459**, 820 (2009).
 - [68] C.-H. Park and S. G. Louie, Nano Lett. **10**, 426 (2010).